A crystal engineering approach for rational design of curcumin crystals for Pickering stabilization of emulsions

(Article begins on next page)

19 October 2024

1 # A crystal engineering approach for rational design of curcumin

2 # crystals for Pickering stabilization of emulsions

3 *Giulia Del Duca[1], Emmanuele Parisi[1], Fiora Artusio[1], Eleonora Calì[1], Silvia Fraterrigo Garofalo[1], Chiara*

4 *Rosso[2], Valentina Cauda[1], Michele Remo Chierotti[2], Elena Simone[1]**

5 *Affiliations*

6 *1 Department of Applied Science and Technology (DISAT), Politecnico di Torino,10129 Torino, Italy*

7 *2 Dipartimento di Chimica I.F.M, Università degli Studi di Torino, 10125, Torino, Italy*

8 **Corresponding author: elena.simone@polito.it*

10

11 # Abstract

12 Emulsions stabilized via Pickering particles are becoming more and more popular due to their high

13 stability and biocompatibility. Hence, developing new ways to produce effective Pickering particles

14 is essential. In this work, we present a crystal engineering approach to obtain precise control over

15 particle properties such as size, shape, and crystal structures, which may affect wettability and

16 surface chemistry. A highly reproducible synthesis method via anti-solvent crystallization was

17 developed to produce submicron-sized curcumin crystals of the metastable Form III, to be used as

18 Pickering stabilizers. The produced crystals presented a clear hydrophobic nature, which was

19 demonstrated by their preference to stabilize water-in-oil (W/O) emulsions. A comprehensive

20 experimental and computational characterization of curcumin crystals was performed to rationalize

21 its hydrophobic nature. Analytical techniques including Raman spectroscopy, powder X-ray

22 diffraction (PXRD), Solid-State Nuclear Magnetic Resonance (SSNMR), scanning electron microscopy

23 (SEM), Differential Scanning Calorimetry (DSC), confocal fluorescence microscopy and contact angle

24 measurements were used to characterize curcumin particles in terms of shape, size and interfacial

25 activity. The attachment energy model was instead applied to study relevant, surface properties of

26 curcumin crystals, such as topology and facet-specific surface chemistry. This work contributes to

27 the understanding of the effect of crystal properties on the mechanism of Pickering stabilization and

28   paves the way for the formulation of innovative products in fields ranging from pharmaceuticals to

29   food science.

30

Introduction

32   Nowadays, emulsions are widely used in the food and pharmaceutical industries for encapsulation,

33   controlled release, and delivery of active compounds (Chen et al., 2020; Frelichowska et al., 2009;

34   Tan & McClements, 2021; Tang et al., 2015).

35   In recent years, there has been a growing interest in Pickering systems (Dickinson, 2010; Ewens et

36   al., 2021; Metilli et al., 2022; Yang et al., 2017), a specific type of emulsion stabilized by solid

37   particles, which irreversibly adsorb at the interface between two immiscible phases (Chevalier &

38   Bolzinger, 2013). The use of solid particles to stabilize interfaces offers more appealing properties

39   compared to synthetic surfactants (Binks, 2002); in fact, Pickering systems present lower tendency

40   to coalescence of the dispersed phase, higher mechanical resistance and enhanced thermodynamic

41   stability (Albert et al., 2019; Aveyard et al., 2003). Additionally, food-grade particles derived from

42   natural sources can be used as stabilizers for food, pharmaceutical and agrochemical applications.

43   Compared to traditional stabilizers food-grade, natural particles are more sustainable, less toxic,

44   more biocompatible and are associated to less negative side effects like irritation and allergies (Tang

45   et al., 2015).

46   The formation mechanism, thermodynamic stability, and functionality of Pickering emulsions are

47   influenced by many factors, including particle wettability, size, and morphology (e.g., aspect ratio)

48   distributions (Pugh, 2016; Wu & Ma, 2016; Xia et al., 2021). Therefore, a correct design of crystalline

49   particles and the related production processes is crucial to obtain the desired multiphase system

50   performance.

51   The type of emulsion stabilized by Pickering particles, whether oil-in-water (O/W) or water-in-oil

52   (W/O), is influenced by the surface nature of Pickering particles. This is often described by the three-

53   phase contact angle (θ) formed between the solid particle and the oil/water interface. When the

54   angle formed on the water side (θ_w) is less than 90°, particles are more suitable for the stabilization

55   of O/W emulsions. On the contrary, when this contact angle exceeds 90°, the formation of W/O

56   emulsion is more favoured (Binks & Lumsdon, 2000).

The size distribution of Pickering particles also influences directly the average size of emulsion droplets formed during emulsification. Typically, Pickering particles are at least one order of magnitude smaller than the average size of emulsion droplets (Xia et al., 2021). Particle morphology (e.g., aspect ratio) was also found to have an effect on Pickering stabilization; particles characterized by a high value of aspect ratio, such as ellipsoids, fibres and rods, were found to better stabilize emulsion droplets compared to more spherical shapes (Jafari et al., 2020).

A variety of plant-derived particles, such as polysaccharides (e.g., cellulose, starch, chitosan), proteins, and polyphenol crystals (Luo et al., 2011), can be utilized to stabilize emulsions. Crystalline polyphenols, including curcumin, are particularly attractive due to their edibility, cost-effectiveness, and health benefits (Xiao et al., 2021). Curcumin is one of the most recently studied compounds (Nelson et al., 2017), which also exhibits surface activity (Sarkar & Dickinson, 2020; Zembyla et al., 2020)(Aditya et al., 2017; Zembyla et al., 2018, 2019). Furthermore, curcumin has a high tendency to arrange in different crystal structures, such as polymorphs or co-crystals (Sanphui & Bolla, 2018). Polymorphs and co-crystals of the same compound can present different bulk properties such as solubility, thermodynamic stability, and dissolution rate; but also different surface features (i.e., roughness and chemical nature), which can be rationally linked with crystal structure properties (Klitou et al., 2022, 2023) (Prandini et al., 2024; Preston et al., 2024).

In this work, a crystal engineering approach was used to develop a robust methodology for the synthesis of sub-micron curcumin particles suitable for Pickering stabilization. In particular, crystal engineering tools such as molecular modelling (e.g., Particle Informatics) and multi-technique particle characterization techniques (e.g., SEM, DSC, XRD) were used to relate crystal structure with important Pickering properties such as roughness and surface chemistry (Desiraju, 2013).

Curcumin crystals were obtained by anti-solvent crystallization, a technique that offers better control over crystal size and shape distribution compared to classical top-down methodologies such as micronization (e.g., jet or ball milling). Additionally, anti-solvent crystallization prevents the formation of amorphous, unstable particles, (Thorat & Dalvi, 2012) and favours the growth of crystals with narrow size and shape distributions. On the other hand, anti-solvent crystallization processes make use or organic solvents, which usually needs to be separated from the anti-solvent (e.g., via distillation) after particles have formed. Additionally, this particle production technique requires further unit operations such as filtration or centrifugation to separate solid particles from the mother liquor.

Following another typical crystal engineering approach (Simone et al., 2015; Simone & Nagy, 2015), we performed a systematic investigation of the relationship between crystallization conditions (e.g., stirring rate, ratio solvent to anti-solvent, volume and concentration) and curcumin crystal shape (aspect ratio), size and polymorphism using Design of Experiment (DoE). Finally, interfacial properties of curcumin crystals were studied with contact angle measurements, emulsification experiments and confocal fluorescence microscopy. This work highlights a clear relationship between crystal properties of curcumin particles (size, shape, polymorphic form) and their ability to act as Pickering stabilizer, showing that a crystal engineering approach can be effective in the design of Pickering particles and the processes necessary to produce them.

1. Materials and Methods

Curcumin from turmeric rhizome (98 wt% total curcuminoid content, >78 wt % curcumin) was obtained from Thermo Fisher Scientific. Ethanol (99.98%) was purchased from Sigma-Aldrich. Medium-chain triglycerides (MCT) oils (Nature Aid) was purchased from a local store. Water purified by treatment with a Milli-Q apparatus was used for all the experiments. The curcuminoid mixture was used without further purification and will be referred to as raw curcumin from now on in this paper. The presence of structurally related impurities (*Figure 1*) is not a limitation for the purpose of this work. Curcumin molecules in the crystal lattice mainly interact via hydrogen bonding interactions that do not involve the methoxy groups; these are not even involved in any significant intramolecular interaction that can be responsible for molecular torsion (Heffernan et al., 2018). Thus, the presence of a high concentration of demethoxycurcumin incorporated in the crystal structure does not greatly affect the properties of the powder.

1.1 Solubility measurement in Ethanol

The solubility of curcumin as purchased (Form I) in ethanol was determined using the Crystal 16 apparatus (Technobis). Curcumin was previously gently ground in a mortar using an agate pestle, then weighed and dispersed in ethanol in a 1.5 mL vial. 12 different concentrations were prepared. Bottom stirring at a fixed speed of 780 rpm was used to keep the particles well dispersed. The samples underwent three consecutive dissolution and recrystallization cycles, by changing temperature from 0 °C to 70 °C, with a heating rate of 0.3 °C/min and a cooling rate of -0.3 °C/min.

1.2 Solubility measurement in ethanol-water mixtures

Raw curcumin in ethanol-water mixtures in different ratios was quantified with a high-performance liquid chromatography (HPLC) system (Shimadzu 20A Nexera). A Kinetex core shell C18 column (5 µm, 150 × 4.6 mm) by Phenomenex and a photo diode array detector were employed to quantify the solute dissolved in the mixtures. Curcumin and solvents absorbance was previously evaluated; 425 nm wavelenght was selected. The mobile phase used consisted of acetonitrile and 0.1% formic acid at a ratio of 50/50 (v/v). The analytes were eluted using a isocratic elution method with a flow rate maintained at 0.8 mL/min, and the column oven temperature fixed at 40 °C. The injection volume was set at 10 µL (Peram et al., 2017). The calibration curve was obtained starting from a series of standard solutions of raw curcumin in ethanol with varying concentrations from 0.1 µg/mL to 100.0 µg/mL, obtained by serial dilutions from the 100.0 µg/mL ethanolic stock solution. A total of nine points were collected in duplicate. The quantification of curcumin dissolved in ethanol-water mixtures with increasing water content (ratio ranging from 1:2.5 to 1:20 w/w) was determined by interpolation from the calibration curve. The analyte composition of the solvent had no significant effect on the precision of the calibration method. The analyte samples were prepared stirring for 15 minutes an excess of raw curcumin in the ethanol-water mixtures. . The excess precipitate was allowed to settle and the dispersions were filtered using a 22 µm syringe filter. The resulting solutions were then placed in HPLC vials for quantification. The measurements were conducted in triplicate.

1.3 Anti-solvent crystallization experiments

Anti-solvent precipitation experiments were designed considering different operating conditions, namely the concentration of curcumin in the ethanolic solution, the ethanol-water ratio, the final volume of the crystallization solution, and the speed of stirring during the anti-solvent addition. A Design of Experiment (DoE) approach was used to plan a set of experiments varying these four different factors. Five different levels for each factor were considered (*Supporting Info Table S1*). The experimental matrix was generated using the default *ccdesign* function in MATLAB R2021a. A statistical analysis of the effect of these different experimental factors (and their combinations) on particle average size and aspect ratio was conducted using the Chemometric Agile Tool (CAT) 3.1.2 software, freely available from https://www.gruppochemiometria.it/f following the approach shown by (Leardi, 2009).

| Codice campo modificato |

146   *Table 1* lists the conditions selected for each experiment. Raw curcumin was weighed and solubilized

147   in ethanol (solvent). The curcumin ethanolic solution was then rapidly mixed with Milli-Q water (anti-

148   solvent) at room temperature in a 1 L beaker in one step addition. While pouring the ethanolic

149   solution, the water was stirred using an Ultra-Turrax (IKA) device to create homogeneous

150   supersaturation. The mixture was stirred an additional 5 min to ensure equilibrium after the

151   curcumin crystal precipitation. The resulting dispersion was filtered under vacuum using a Büchner

152   flask, funnel, and filter paper (90 mm diameter) to separate the particles formed from the solvent

153   mixture. The filter cake was washed with water and completely dried in open air for 24 hours. Both

154   the curcumin raw material and curcumin recrystallized powders obtained (named curcumin

155   recrystallized from now on in this paper) have been subjected to extensive characterization.

156   ### 1.4 Characterization of curcumin crystals

157   **Raman Microscopy:** To check the homogeneity of the curcumin recrystallized powders, Raman

158   spectra and spatial maps were acquired at room temperature using a confocal Raman microscope

159   Horiba LabRAM HR Evolution. A 785 nm laser was used as the excitation source, and the Raman

160   signal was collected with a Synapse Plus BIDD Detector (1024 x256 pixels), utilizing a 300/nm grating.

161   No filter was applied and the laser power was set at 50%. Several milligrams of material were placed

162   on a glass slide, the powder was pressed and scanned in a grid pattern using the 5X objective. The

163   sampling parameters were set to get 5 acquisitions with an exposure time of 0.5 s, and a total of 100

164   points were measured for each sample.

165   To check the kinetic stability of the recrystallized powder in water, a total of 150 mg of recrystallized

166   curcumin was dispersed in 200 mL of Milli-Q water in a 250 mL graduated jacketed reactor. The

167   dispersion was maintained in agitation using magnetic stirring at 400 rpm for 63 hours. A Huber

168   Ministat 230 (Huber, Germany) was used to control and maintain the temperature constant at 25 °C.

169   The dispersion was monitored in situ using a fiber-optic SuperHead Raman probe, with a 785 nm

170   laser as the excitation source, connected to the Horiba LabRam mentioned earlier. To prevent

171   interference from external light, the slurry, and the probe were covered in aluminium foil. One

172   spectrum was recorded every hour, to monitor possible changes in solid form. The acquisition

173   parameters were set to collect 20 acquisitions with 10 s exposure time. The effects of cosmic rays in

174   the spectra were manually removed.

175 **_Powder X-ray Diffraction (PXRD):_** PXRD analysis was performed using a Panalytical X'Pert PRO
176 diffractometer set up in Bragg–Brentano mode with Cu Kα radiation (λ = 1.5406 Å). The samples
177 were gently ground in a mortar with an agate pestle and loaded onto a silicon zero-background
178 sample holder, and diffraction patterns were recorded over a 2θ range of 4° to 40° with a step size
179 of 0.026° and an acquisition time of 180 seconds per step. The obtained diffraction patterns were
180 compared with the simulated X-ray patterns obtained from the polymorphs crystal structures
181 deposited in the Cambridge Structural Database (CSD), refcodes BINMEQ13, BINMEQ12 and
182 BINMEQ07 for form I, II and III, respectively.

183 **_Solid-State Nuclear Magnetic Resonance (SSNMR):_** ^{13}C CPMAS (_Cross-Polarization Magic Angle_
184 _Spinning_) SSNMR spectra were acquired with a Bruker Avance II 400 Ultra Shield instrument,
185 operating at 400.23 MHz for ^{1}H and 100.63 MHz for ^{13}C. The powder samples were packed into
186 cylindrical zirconia rotors with a 4 mm o.d. and 80 µL volume without further preparations or
187 treatments. ^{13}C spectra were acquired at room temperature at a spinning speed of 12 kHz using a
188 ramp cross polarization (CP) pulse sequence with a 90° ^{1}H pulse of 3.8 µs, a contact time of 3 ms,
189 optimized recycle delays of 3.94 and 3.6 s for raw curcumin and the recrystallized sample
190 respectively, and a number of scans equal to 1000. The two-pulse phase modulation (TPPM) scheme
191 was used for heteronuclear decoupling, with a radio frequency field of 65.8 kHz. The ^{13}C chemical
192 shift scale was calibrated through the methyl signal of the external standard adamantane (at 38.48
193 ppm with respect to tetramethyl silane, TMS).

194 **_Differential Scanning Calorimetry (DSC):_** DSC analysis was performed using a Mettler Toledo
195 8000 DSC-1 calorimeter. Approximately 2.5 mg of each sample was placed in a 40 µL aluminium pan,
196 covered with a perforated lid. The samples were heated from 25 °C to 185°C at a heating rate of 10
197 °C/min under a nitrogen atmosphere and then cooled to 20 °C, at a cooling rate of 10 °C/min.

198 **_Scanning Electron Microscopy (SEM):_** The crystal morphology and particle size distribution of the
199 recrystallized curcumin samples were assessed through image analysis obtained with a Zeiss Merlin
200 Field Emission Gun Scanning Electron Microscope. Dry particles were finely dispersed using a spatula
201 then fixed onto SEM specimen stubs. A platinum coating was deposited to improve sample
202 conductivity for better image quality. The coating procedure lasted for 30 s at 30 mA.The acquired
203 SEM images were subjected to analysis using ImageJ 1.54g software. Images were manually
204 segmented. Binarization was applied to convert the images into binary format, and the dimensions
205 (length and width) of the particles were obtained through the software. Due to the needle-like/rod-

206 shaped morphology of the particles, an ellipse was fitted to each particle (ImageJ default function

207 "Fit ellipse"), and the minimum and maximum lengths were considered to calculate the aspect ratio

208 and Feret's diameter (called equivalent diameter from now on). An example of the workflow used

209 for image analysis is shown in *Supporting Info Figure S1*. To ensure statistical reliability, a minimum

210 of 300 particles were selected for each sample as shown in *Supporting Info Table S2*.

211 *1.5 Computational analysis of curcumin crystal structures*

212 The crystallographic information files (.cif) for the two curcumin polymorphs structures (form I and

213 form III) used in the analysis were obtained from the Cambridge Structural Database (CSD), refcode

214 BINMEQ13 for form I, refcode BINMEQ07 for form III. The .cif files were analyzed with the CCDC

215 Mercury software v.2023.1.0 (Macrae et al., 2008). The optimization of the crystal structures was

216 performed using Materials Studio 2021 (v 21.1.1.3268). Geometry optimization was carried out with

217 the Forcite algorithm with Dreiding force field (Liu et al., 2019). The crystal habit of the curcumin

218 polymorphs was predicted by the growth morphology method, which gave several possible crystal

219 faces. The crystals were sliced parallel to the morphologically important surfaces (h k l) with a depth

220 of 2 × dhkl. A crystal segment was created as a periodic superstructure of 3 × 3 unit cells. The

221 interactions between the molecules in the unit cell were calculated with the Crystal Graph tool of

222 the morphology module in Material Studio that ranks the intermolecular interactions. Thus, the

223 fastest growth rate of the crystal surface would be present in the direction that contains the

224 strongest interactions, which means that the curcumin molecules grow faster along the strongest

225 interaction. The crystal surfaces that have a fast growth rate will vanish and the crystal surfaces with

226 a slow growth rate will appear in the final morphology. The surface analysis of the crystal facets of

227 the two polymorphs was performed with CSD-particle tool in Mercury to study the surface

228 roughness of the most dominant facets.

229 *1.6 Contact Angle Measurements*

230 The wettability of both the raw curcumin and the crystallized particles was evaluated by measuring

231 the contact angle through sessile drop technique using a DSA25 Drop Shape Analyzer (Krüss

232 Scientific) equipped with a microsyringe and CF03 high-speed camera with CMOS sensor. Water at

233 different pH (pH 7 and 3) and medium-chain triglyceride (MCT) oil were tested on a disk of curcumin

234 pressed powder. Disks of approximately 100 mg were prepared by placing gently ground powder

235 between the plates of a hydraulic bench press with a diameter of 1.2 cm and pressing the sample

under a pressure of 200 bar for 30 seconds. Two trace paper disks were inserted between the plates to ensure the formation of a homogeneous and smooth disc surface. The measurements were conducted at room temperature. Water and oil droplets (2 μL droplet volume) were placed onto the disk surface using a needle, and the droplet behavior was recorded with a camera. The droplet contour was analysed using the Young-Laplace method with Krüss Advance 1.12.0.35401 software, and the contact angle between the disk substrate and the water (θ_1) or oil droplet (θ_2) determined. Each measurement was performed five times to ensure accuracy. The three phase contact angle curcumin, oil and water (θ_3) was calculated from these two values using the following equations (referring to the schematic of Figure 2):

$$\gamma_{CA} - \gamma_{CW} - \gamma_{AW} \cos \theta_1 = 0$$

$$\gamma_{CA} - \gamma_{CO} - \gamma_{AO} \cos \theta_2 = 0$$

$$\gamma_{CW} - \gamma_{CO} - \gamma_{WO} \cos \theta_3 = 0$$

where the σ values are the surface tensions among the different phases: air (A), curcumin (C) and water (W). Most of these values were taken from literature and are respectively: $\gamma_{AO} = 30.14\ mN/m$, $\gamma_{AW} = 72.8\ mN/m$ and $\gamma_{OW} = 24.77\ mN/m$. Rearranging the three previous equations we can obtain the desired value θ_3:

$$\cos \theta_3 = \frac{\gamma_{AO} \cos \theta_2 - \gamma_{AW} \cos \theta_1}{\gamma_{WO}}$$

Commentato [ES1]: @Giulia: Inserire le references per i valori di tensioni interfacciale

1.7 Emulsions preparation and characterization

Preparation of W/O emulsions: Water in oil (W/O) emulsions were prepared using the conditions shown in *Table 3*. The curcumin particle concentration was fixed, while the effect of different amounts of water, the pH and the speed of stirring was tested. Curcumin recrystalized particles were first dispersed in the continuous phase, MCT oil, using the Ultra-Turrax mixer, operating at 10000 rpm for 3 minutes. Water was then added as the dispersed phase, at pH 7 and 3. Two different pH values, pH 3 and pH 7, were tested to appreciate differences in the interface stabilization of curcumin particles. The pH values were chosen to keep the product safe for human consumption. pH >7 was not considered as curcumin undergoes chemical degradation at basic environment (Priyadarsini, 2009). The aqueous phase was mixed with the oil dispersion for 1 minute (experimental conditions in *Table 2*). After preparation, the emulsions were sealed with Parafilm and stored at room temperature in a dark place. For the preparation of the emulsions, both for W/O and O/W, curcumin

9

crystals from experiments 13,14, 15 and 16 reported in *Table 1* were used. Although the characterization of the samples revealed no significant differences between the batches, the samples were selected because they were the most similar in terms of mean value of particle size, aspect ratio and morphology.

Preparation of O/W emulsions: Recrystallized curcumin powder was dispersed in the continuous phase (Milli-Q Water), followed by the addition of the dispersed phase (MCT oil), and the system was further mixed for several minutes. The pH of the acidic water was adjusted by adding a few drops of an aqueous solution of 0.1 M HCl. Different dispersing and emulsification methods, such as Ultra-Turrax mixing, ultrasound bath and handshaking, were tested, curcumin crystals load and amount of oil were evaluated, as reported in *Table 3*. The emulsions were sealed with Parafilm and stored at room temperature in a dark place.

Characterization and stability assessment of curcumin emulsions: Optical microscopy was used to measure the size distribution of the dispersed phase in the emulsions prepared with curcumin crystals. A Zeiss Axiolab 5 microscope at 5X and 10X magnifications was used for this purpose; images were collected with a digital camera with 48 Mp, resolution 4000 x 3000 pixels. The images collected were analysed using ImageJ version 1.52g, as described above for the crystal size distribution measurements with SEM. For each sample, the Feret diameter of 100 droplets minimum were considered.

To examine the structure of both water-in-oil (W/O) and oil-in-water (O/W) emulsion droplets, a spinning disk confocal microscope (Nikon Eclipse Ti-e fluorescence optical inverted microscope) was utilized, equipped with crest large FOV lasers and a super bright wide-spectrum source (Shutter Lambda XL), a high-resolution camera (Zyla 4.2 Plus, 4098 × 3264 pixels, Andor Technology), and a motorized stage. 10 µL of the sample was carefully placed onto a glass slide, ensuring the absence of any air gaps between the sample and the coverslip. The emulsions were gently agitated before the measurement to ensure homogeneity. Brightfield, green and red emission images, recorded with a light excitation of 488 nm and 550 nm, respectively, were acquired using a 20x objective (Nikon). In order to assess the stability against coalescence of the prepared emulsions, all samples were kept at room temperature and protected from light for several months. Samples were periodically checked visually to observed phase separation and with optical microscopy to quantify droplet size distribution.

295

2. . *RESULTS & DISCUSSION*

2.1 Curcumin crystals preparation and characterization

Sub-micrometer curcumin crystals were successfully produced via anti-solvent crystallization. The chosen anti-solvent technique and the parameters tested aimed to maximize supersaturation conditions, promoting nucleation over growth (Meenan, 2001), and yielding small crystals with narrow size distribution. A high yield of recovery from the liquid, ranging from 80% to 94% w/w (ratio between starting material weight and recovered powder weight) was also favoured with this method (data in *Supporting Info, Table S3*). To define the crystallization parameters to test, in terms of solute concentration and solvent-antisolvent ratio, previous solubility measurements of curcumin in ethanol and in ethanol-water analytes with increasing water content were performed. *Figure 3 a and b* show respectively the solubility of raw curcumin in ethanol at different temperatures (ter Horst et al., 2009) and the solubility of curcumin in ethanol-water mixtures. Further information related to this data is shown in *Supporting Information Figure S2*. Upon resuspension in water of the obtained crystals, a fine, homogeneous, dispersion was formed, with a considerable improvement in ease of dispersion compared to the raw curcumin. To confirm the absence of chemical degradation or amorphization during particle formation and identify the crystal form, various analytical techniques, including Raman spectroscopy, powder X-ray diffraction (PXRD), Solid-State Nuclear Magnetic Resonance (SSNMR) and Differential Scanning Calorimetry (DSC) were used. The analyses were conducted on the recrystallized samples and the raw untreated material. The particle morphology and size distribution were evaluated through SEM imaging.

Various characterization techniques, including Raman spectroscopy, PXRD, SSNMR and DSC were performed on each crystallized sample to determine crystallinity, polymorphic form, and thermal properties. The polymorphic form of the crystals obtained via anti-solvent precipitation experiments was always the metastable form III of curcumin (Thorat & Dalvi, 2014). This metastable form formation is favoured by the high supersaturation achieved at high water to ethanol solution ratios (Coquerel, 2014; Roelands et al., 2006) and with the rapid mixing provided by the UltraTurrax. The crystallized material exhibited a characteristic red-orange colour compared to the yellow-orange of the raw curcumin (*Supporting Info, Figure S3*), which was found to be stable Form I of curcumin.

11

324   The formation of polymorph form III was confirmed by PXRD analysis and comparing the collected

325   powder patterns to the calculated ones from crystallographic data from literature (*Figure 4*). The

326   PXRD diffractograms show high crystallinity (e.g., sharp peaks) of the curcumin particles from anti-

327   solvent precipitation, and homogeneity in terms of polymorphism. DSC thermograms of raw and

328   recrystallized curcumin (form I and form III) are presented in *Figure 5*. Form I exhibits an endothermic

329   peak at 178°C, corresponding to melting of the sample. In the thermogram of form III, the first peak

330   at 161°C corresponds to an endothermic solid-state transformation to form I, as confirmed by other

331   studies (Pandey & Dalvi, 2019; Thorat & Dalvi, 2015). The second endothermic peak at 179.5 °C

332   corresponds to the melting of form I (Sanphui et al., 2011; Thorat & Dalvi, 2015). The slightly

333   different onset of melting between the two samples can be attributed to the different particle sizes

334   (Lee et al., 2001).

335   Due to the high similarity between the diffraction patterns of curcumin form II and III (Sanphui et al.,

336   2011), SSNMR analysis was also performed to further confirm the polymorphic form of the anti-

337   solvent curcumin crystals. This solid-state characterization technique allows discerning different

338   crystalline forms with great accuracy due to its high sensitivity to the chemical surroundings of the

339   nuclei constituting the system (Chierotti et al., 2010).

340   The most important structural difference between forms II and III is the number of independent

341   molecules: one for the latter (Z = 8, Z' = 1), as in form I, and two for form II (Z = 8, Z' = 2), making

342   them easily distinguishable by SSNMR (Dai et al., 2020). In fact, Z' = 2 results in a splitting of all signals

343   in the spectrum, except for some casual overlapping. *Figure 6* shows the ^{13}C CPMAS SSNMR spectra

344   of raw and recrystallized curcumin.

345   Only two signals can be observed for C2 and C2' (*Figure 1*). More than any others these signals allow

346   a distinction between the different polymorphic forms: for raw curcumin they are found at 187.1

347   and 182.6 ppm, while for recrystallized curcumin at 188.9 and 177.9 ppm. These results are in good

348   agreement with what have been reported in the literature for form I and III, respectively (*Table 4*)

349   (Dai et al., 2020), indicating that the raw curcumin mainly consists of curcumin form I, while the

350   recrystallized one of form III. The presence of single signals for the two expected C atoms in this

351   region definitively rules out the formation of form II, for which a number of signals of four, two for

352   C2 and two for C2', is expected. However, spurious signals are observed in both 13C CPMAS spectra:

353   at 184.9 ppm and at 158.8 ppm for raw curcumin and at 158.4 ppm for the recrystallized one. These

354   impurities are likely due to the presence of curcumin derivatives, such as demethoxycurcumin and

12

bisdemethoxycucrcumin (Siudem et al., 2023). As mentioned earlier, given the absence of involvement of curcumin methoxy groups in H-bonds or significant intramolecular interaction that can be responsible for molecular torsion, the presence of these derivatives does not affect greatly the properties of the compound.

Raman microscopy was used to obtain 2D maps of all the curcumin crystals obtained via anti-solvent precipitation to verify the homogeneity of the samples. *Figure 7* shows the Raman spectra of monoclinic form I and orthorhombic form III. The latter exhibits a unique peak at 1532 cm^{-1}, corresponding to intermolecular interactions in the central keto-enol region. Form I shows enhanced ν(C=C) stretching vibrations. These two peaks were used to unequivocally identify the two forms (Prasad et al., 2020) in each collected map. All samples were found to be homogenous in terms of polymorphism, with only form III detected in all spectra collected for each map (example of measurement shown in *Supporting Info, Figure S3*).

As the recrystallized Form III is thermodynamic unstable at ambient conditions we checked for its kinetic stability (e.g., slow kinetic of polymorphic transformation) in air and water. In fact, a kinetically stable solid can still be used for Pickering formulations. Form III samples did not show polymorphic changes when stored at room conditions in a dark place for over 10 months. In situ Raman was used to check kinetic stability of Form III in water slurry; Figure 8 shows that no significant differences in Raman spectra were observed over the 63 hr of the experiment, indicating the absence of phase transformation or degradation of curcumin crystals. Slurries of curcumin in water were further check after 3 months and show the persistence of Form III. Therefore, it can be concluded that form III has reasonable kinetic stability and may be used in Pickering formulations with long shelf-life .

SEM images of recrystallized curcumin particles obtained from one batch (Exp 1 reported in *Table 1*) are reported in Figure 9. Crystals show fairly narrow size and shape distributions, predominantly exhibiting a needle/rod-like shape (Figure 9a-b). Additionally, aggregates of crystals can be observed, potentially formed during filtration. Furthermore, dendritic structures (*Figure 9c-d*) can be observed, likely formed due to secondary nucleation, which is influenced by the mixing conditions and the level of supersaturation used during the experiments. The high-speed rotor-stator mixing employed in this study generates shear forces and turbulent flow, facilitating mixing and mass transfer but also leading to crystal breakage or aggregation (*Figure 9c-d*). Fragile crystals that grew as dendrites or needles were more prone to breakage into smaller particles.

13

Quantification of morphology (aspect ratio) and size distributions of crystallized curcumin particles were determined by examining SEM images at various magnifications for all 25 samples. The results for a representative experiment are graphically shown in *Figure 10 (Exp 1 of Table 1); whereas* the average size and aspect ratio values with their standard deviation are reported in Supporting Information Table S3. The crystallized samples exhibited a narrow distribution of equivalent diameters, ranging from 0.5 to 1.2 μm, with a mean aspect ratio ranging from 1.6 to 3.5. Supporting Information *Figure S4* shows the results of the statistical analysis performed on the size and shape average values; this analysis demonstrates that there is no significant relationship between operating parameters (e.g., stirring rate, volume ratio) explored and the resulting particle size and morphology, within the chosen design space. This might be related to the fact that similar, high levels of curcumin supersaturations were used in all experiments, despite changes in solvent to antisolvent ratios and curcumin initial concentrations. At such high levels of supersaturations, it is possible that the effect of other operating conditions on crystal size and shape distributions might be negligible.

A noticeable reduction in particle size was observed when comparing the shape and size of the curcumin crystallized via anti-solvent with the raw material provided by the supplier (mean equivalent diameter of 3.8 μm and mean aspect ratio of 1.4). Additionally, the higher average aspect ratio in the recrystallized samples indicated a more acicular shape compared of anti-solvent crystallized curcumin compared to the raw material.

The interfacial behaviour of curcumin particles (raw and from anti-solvent crystallization) was determined through contact angle measurements (θ_1 and θ_2), which are reported in Table 6. Curcumin raw powder (form I) showed a hydrophobic nature with a value of θ_1 of around 90°, and more affinity with the oil phase (θ_2 around 29°). The recrystallized form III has similar affinity to oil (θ_2 is about 24°) but shows a more hydrophilic nature with an average value of θ_1 of 62.4°. Non-significant differences in values of θ_1 were observed with water at different values of pH. The values of measured contact angle explain the better dispersibility of the recrystallized Form III in water, compared with the raw Form I material. The minimum calculated θ_3 value (considering the measurement standard deviation) for Form I at pH=7 is around 36°, which indicates suitability for water in oil emulsion stabilization. The θ_3 value for the recrystallized curcumin ranges from 81 to 124°, which indicates the potential of curcumin particles for stabilization of both O/W and W/O emulsions. It is worth noticing the considerably higher standard deviation of the measurements conducted on Form III in water compared to Form I. This might be related to the smaller size of the

417 recrystallized particles, which significantly affected the quality of the compressed disk (e.g., higher
418 surface roughness, difficulties in powder handling). Despite the larger standard deviation, the higher
419 hydrophilicity of form III is evident. This is likely related to the different molecular termination
420 characterizing the facets of the two curcumin polymorphs. In fact, different polymorphs of the same
421 compound can expose different functional groups of their constituting molecules on their facets,
422 affecting facet-specific surface properties. Additionally, it has been reported that polymorphs usually
423 differ in surface roughness (Montis et al., 2020), which can also affect wettability. To verify this
424 hypothesis a computational study of the two crystal structures was performed using Mercury and
425 Materials Studio. *Figure 11* shows the predicted morphology of curcumin form I and form III (*Figure*
426 *11 a* and *b*) and a graphical representation of the topology for the largest facets identified (*Figure 11*
427 *c* and *d*). As visible from *Table 5*, both the polymorphs show a high contribution of the van der Waals
428 interactions (*i.e. π-π* stacking) for all the crystal facets. The contribution of the hydrogen bond and
429 electrostatic interactions to the total lattice energy is minimal for Form I. Indeed, as shown in *Figure*
430 *11 a*, neither of the facets' termination show any hydrogen bond acceptor or donor groups (*e.g.*
431 methoxy and hydroxy groups). On the other hand, curcumin form III shows a slightly higher
432 contribution of both hydrogen bond and electrostatic interactions to the total lattice energy; this is
433 demonstrated by the presence of hydrogen acceptor and donor groups on the most of Form III facets
434 (*Figure 11 b*). Comparing the two topologies (*Figure 11 c* and *d*) form III presents a higher surface
435 roughness compared to Form I (more details are given in *Supporting Info Figure S6* and *Figure S7)*.
436 The computational analysis is, therefore, in agreement with the experimental data that indicates a
437 more hydrophilic nature of curcumin form III compared to form I.

2.4 Emulsions preparation and characterization

439 Water-in-oil (W/O) emulsions were prepared using the conditions reported in Table 3. Figure 12
440 shows the visual appearance of the prepared emulsions, which did not show evident phase
441 separation for solid particles and the two liquid phases. It is worth noticing that water droplet
442 sedimentation was observed within a few minutes of preparation of the W/O emulsions due to the
443 large average size the dispersed phase. Confocal fluorescence microscopy of the samples was
444 performed to check the type of the formed emulsion and to assess the interfacial activity of
445 curcumin particles. Figure 13 clearly shows that a Pickering stabilized W/O emulsion is formed; water

15

446 droplets are surrounded by curcumin particles adsorbed at the water/oil interface. The yellow color

447 is due to the colocalization of curcumin emitting both in the green channel, when dissolved in MCT

448 oil, and in the red channel as solid phase. It is worth noticing that neither MCT oil nor water were

449 stained with other dyes, hence the natural green fluorescence is due to dissolved curcumin.). The

450 arrangement of curcumin particles around the water droplets indicates the typical droplet bridging

451 of Pickering emulsions (French et al., 2015), which provides improved stability to the droplets and

452 reduces coalescence over time.

453 The size distribution of water droplets in each emulsion sample was measured via optical light

454 microscopy. All droplet size distributions are reported in Figure 14; whereas the average values with

455 corresponding standard deviations are reported in Table 7. Water droplets were found to be

456 between 70 to around 100 μm in equivalent diameter, which is consistent with the mean size of the

457 curcumin particles used. It can be observed that higher contents of water in the emulsions

458 determined higher average droplet sizes and improved interfacial coverage by particles (as shown

459 more clearly in *Figure 15 m-n-o-p*). In general, all droplet size distributions are quite broad, as shown

460 by the relatively large standard deviations ranging from 30 to over 100 μm. Increasingly broader

461 droplet size distribution can be observed as the amount of dispersed phase in the emulsions

462 increases, as clearly shown in Figure 14 a to c. Nevertheless, the presence of there smaller droplets

463 is beneficial, as they form a particle/droplet network that provides bulk stabilization to the emulsions

464 via a bridging mechanism (as shown more in details in Supporting Info, Figure S8).

465 The type of stirring had a weak effect on the average size and standard deviation of the droplet

466 distributions; slightly larger and broader distributions were observed with handshaking compared

467 to high-shear mixing (e.g., Emu W/O 1 vs 2, 4 vs 5 and 10 vs 11). However, in Figure 15 it can be

468 observed that an increase in shear resulted in a higher occurrence of droplet bridging, in agreement

469 with previous studies reported by French et al.(French et al., 2015). Additionally, higher shear led to

470 the more uniform surface coverage from the particles and fewer solid particles dispersed in the

16

Commentato [ES2]: @Giulia: inserire references

471 continuous oil phase. These observations are shown more clearly in Figure 15 a to l). The pH of the

472 water phase also influenced the emulsion microstructure. By comparing Emu W/O 1 and 4, and 7

473 and 10 (Figure 14 and Table 7) it is possible to observe the effect of pH on droplet size distribution.

474 Emulsions prepared with lower pH exhibited larger droplets compared to those prepared at pH 7,

475 which is consistent with previous findings of Luo et al. evaluating the efficiency of flavonoids as

476 stabilizers in biphasic systems (Luo et al., 2011).

477 A decrease in pH led to the formation of large aggregates of curcumin particles (*Figures 13 e-f-j-k*,

478 opaque spots), which reduced the number of available particles for interfacial stabilization.

479 Despite the relatively large droplet sizes, the W/O emulsions prepared with curcumin particles did

480 not show significant visual changes over several weeks of storage. A representative example of long-

481 term stability is shown in *Figure 16*, which depicts the appearance of the Emu W/O 16 emulsion four

482 months after preparation.

483 A further demonstration of the interfacial adsorption of curcumin particle in W/O emulsions is

484 shown in *Figure 17*, which shows sample Emu W/O 16 left on a glass for 30 min. The deflated shape

485 of the partially dried water droplets is due to the presence of Pickering particles (Okada et al., 2012),

486 which are strongly adsorbed at the interface and prevent further water diffusion and evaporation by

487 reducing the surface available for mass transfer.

488 Since θ_3 of recrystallized curcumin particles from anti-solvent precipitation was found to be in a

489 range that indicated potential for O/W stabilization, this type of emulsions were also tested.

490 Emulsions were prepared by dispersing recrystallized curcumin particles at different wt % contents,

491 varying the MCT oil wt%, and testing different stirring techniques, as reported in *Table 2.* As shown

492 in Figure 18 the resulting emulsions were unstable, leading to droplet coalescence, phase separation

493 and particle precipitation within a few hours regardless of the different parameters tested. Visual

494 inspection of the vials revealed large droplet sizes (*Figure 18-a*), regardless of the method of

495 preparation and the composition. It is evident that the produced curcumin particles are not suitable

496 for O/W stabilization; indeed a phase inversion was observed in the produced samples

497   (Binks, 2002). Figure 19 shows confocal fluorescence microscope images of the orange, superficial

498 layer visible in the vials of Figure 18a: large oil domains (in green) containing smaller water droplets

499 surrounded by curcumin particles (in yellow at O/W interfaces) are clearly visible. Even though

500 contact angle measurements showed no significant differences in wettability between water at

different pHs, in sample Emu W/O 5.2 (*Figure 18 -b*) where water at pH 3 was used, the preference for curcumin particles to stay in the oil phase was more evident, with all the oil and curcumin particles moving on the top layer. Moreover, no particle precipitation was observed in the water phase when acidic water was used.

3. Conclusions

Crystallization techniques that enable consistent control over particle properties such as size, shape, and polymorphism are essential to produced Pickering formulation with tailored properties for many applications in the food sector. In this study, we applied crystal engineering tools and good practise to develop a robust anti-solvent crystallization method to produce submicron-sized curcumin crystals of suitable for Pickering stabilization. The process developed delivered curcumin particles with a uniform average size (0.5 - 1.2 μm), morphology (rodlike shape), and polymorphic form (the metastable form III). The curcumin particles recrystallized via anti-solvent exhibited improved dispersibility in water and enhanced hydrophilicity compared to the raw material as purchased (stable form I). This is due to the reduced size of the crystallized particles and the facet-specific surface chemistry of curcumin form III, as shown by computational modelling of the two polymorph structures.

Various conditions were investigated in the formulation of O/W and W/O Pickering emulsions, including the water to oil ratio, the type of emulsification technique, and the pH of the water phase. Consistent with the findings of previous studies conducted by Zembyla et al. (Zembyla et al., 2018, 2019), it was observed that curcumin particles provided superior stabilization of W/O emulsions compared to O/W ones. Indeed the O/W samples produced in this work were highly unstable and even show phase inversion. As expected, larger water droplets were observed at higher ratios of water to oil in emulsion, with better particle coverage and bridging phenomenon that provided further bulk stabilization. An increase in the stirring energy provided for emulsification, from handshaking to Ultraturrax mixing, resulted in slightly smaller droplet size. An acidic pH determined droplet enlargement and the formation of large particle aggregates that precipitated; this is probably due to the effect of solution ions on the surface charge of curcumin particles, which can increase particle-particle interactions rather than particle-interface interactions. Despite the formation of relatively coarse emulsions (average droplet diameter up to over 100μm), the particles remained absorbed at the W/O interface, with no phase separation was observed even after 4 months of

18

532 storage. These findings provide a deeper understanding on how crystalline properties, particularly
533 polymorphism, can affect the effectiveness of Pickering particles. The relationship between crystal
534 structure and facet-specific surface chemistry and topology can be predicted with crystal
535 engineering modelling tools; whereas specific crystallization processes can be designed to precisely
536 deliver the desired particle properties. The work presented here is a first example of the application
537 of a crystal engineering approach to rational design of Pickering particles and formulations.

538

Supporting information

540 Further details on Design of Experiment (DoE) and responses analysis, particle size distribution
541 determination, HPLC calibration curve of curcumin ethanolic solution, curcumin crystal simulated
542 facet topology and water-in-oil emulsion details.

543

Acknowledgments

552

553

554 **References**

555 Aditya, N. P., Hamilton, I. E., & Norton, I. T. (2017). Amorphous nano-curcumin stabilized oil in water

556   emulsion: Physico chemical characterization. *Food Chemistry*, *224*, 191–200.

557   https://doi.org/10.1016/j.foodchem.2016.12.082

558 Albert, C., Beladjine, M., Tsapis, N., Fattal, E., Agnely, F., & Huang, N. (2019). Pickering emulsions:

559   Preparation processes, key parameters governing their properties and potential for pharmaceutical

560   applications. *Journal of Controlled Release*, *309*, 302–332.

561   https://doi.org/10.1016/j.jconrel.2019.07.003

562 Aveyard, R., Binks, B. P., & Clint, J. H. (2003). Emulsions stabilised solely by colloidal particles. *Advances in*

563   *Colloid and Interface Science*, *100–102*, 503–546. https://doi.org/10.1016/S0001-8686(02)00069-6

564 Binks, B. P. (2002). Particles as surfactants ˗similarities and differences. *Interface Science*.

565 Binks, B. P., & Lumsdon, S. O. (2000). Influence of Particle Wettability on the Type and Stability of Surfactant-

566   Free Emulsions. *Langmuir*, *16*(23), 8622–8631. https://doi.org/10.1021/la000189s

567 Chen, L., Ao, F., Ge, X., & Shen, W. (2020). Food-Grade Pickering Emulsions: Preparation, Stabilization and

568   Applications. *Molecules*, *25*(14), 3202. https://doi.org/10.3390/molecules25143202

569 Chevalier, Y., & Bolzinger, M.-A. (2013). Emulsions stabilized with solid nanoparticles: Pickering emulsions.

570   *Colloids and Surfaces A: Physicochemical and Engineering Aspects*, *439*, 23–34.

571   https://doi.org/10.1016/j.colsurfa.2013.02.054

572 Chierotti, M. R., Ferrero, L., Garino, N., Gobetto, R., Pellegrino, L., Braga, D., Grepioni, F., & Maini, L. (2010).

573   The Richest Collection of Tautomeric Polymorphs: The Case of 2-Thiobarbituric Acid. *Chemistry – A*

574   *European Journal*, *16*(14), 4347–4358. https://doi.org/10.1002/chem.200902485

575 Coquerel, G. (2014). Crystallization of molecular systems from solution: Phase diagrams, supersaturation

576   and other basic concepts. *Chem. Soc. Rev.*, *43*(7), 2286–2300. https://doi.org/10.1039/C3CS60359H

577 Dai, Y., Terskikh, V., Brinmkmann, A., & Wu, G. (2020). Solid-State 1H, 13C, and 17O NMR Characterization of

578   the Two Uncommon Polymorphs of Curcumin. *Crystal Growth & Design*, *20*(11), 7484–7491.

579   https://doi.org/10.1021/acs.cgd.0c01164

20

580   Desiraju, G. R. (2013). Crystal Engineering: From Molecule to Crystal. *Journal of the American Chemical*

581   *Society*, *135*(27), 9952–9967. https://doi.org/10.1021/ja403264c

582   Dickinson, E. (2010). Food emulsions and foams: Stabilization by particles. *Current Opinion in Colloid &*

583   *Interface Science*, *15*(1–2), 40–49. https://doi.org/10.1016/j.cocis.2009.11.001

584   Ewens, H., Metilli, L., & Simone, E. (2021). Analysis of the effect of recent reformulation strategies on the

585   crystallization behaviour of cocoa butter and the structural properties of chocolate. *Current*

586   *Research in Food Science*, *4*, 105–114. https://doi.org/10.1016/j.crfs.2021.02.009

587   Fang, L., Gao, Z., Gao, Z., Huang, W., Wan, X., Rohani, S., & Gong, J. (2023). Controlled crystallization of

588   metastable polymorphic pharmaceutical: Comparative study of batchwise and continuous tubular

589   crystallizers. *Chemical Engineering Science*, *266*, 118277. https://doi.org/10.1016/j.ces.2022.118277

590   Frelichowska, J., Bolzinger, M.-A., Pelletier, J., Valour, J.-P., & Chevalier, Y. (2009). Topical delivery of lipophilic

591   drugs from o/w Pickering emulsions. *International Journal of Pharmaceutics*, *371*(1–2), 56–63.

592   https://doi.org/10.1016/j.ijpharm.2008.12.017

593   French, D. J., Taylor, P., Fowler, J., & Clegg, P. S. (2015). Making and breaking bridges in a Pickering emulsion.

594   *Journal of Colloid and Interface Science*, *441*, 30–38. https://doi.org/10.1016/j.jcis.2014.11.032

595   Jafari, S. M., Sedaghat Doost, A., Nikbakht Nasrabadi, M., Boostani, S., & Van der Meeren, P. (2020).

596   Phytoparticles for the stabilization of Pickering emulsions in the formulation of novel food colloidal

597   dispersions. *Trends in Food Science & Technology*, *98*, 117–128.

598   https://doi.org/10.1016/j.tifs.2020.02.008

599   Klitou, P., Parisi, E., Bordignon, S., Bravetti, F., Rosbottom, I., Dell'Aera, M., Cuocci, C., Chierotti, M. R.,

600   Altomare, A., & Simone, E. (2023). Navigating the Complex Solid Form Landscape of the Quercetin

601   Flavonoid Molecule. *Crystal Growth & Design*, *23*(8), 6034–6045.

602   https://doi.org/10.1021/acs.cgd.3c00584

603   Klitou, P., Rosbottom, I., Karde, V., Heng, J. Y. Y., & Simone, E. (2022). Relating Crystal Structure to Surface

604   Properties: A Study on Quercetin Solid Forms. *Crystal Growth & Design*, *22*(10), 6103–6113.

605   https://doi.org/10.1021/acs.cgd.2c00707

21

606   Leardi, R. (2009). Experimental design in chemistry: A tutorial. *Analytica Chimica Acta*, *652*(1–2), 161–172.

607   https://doi.org/10.1016/j.aca.2009.06.015

608   Lee, J.-S., Hsu, C.-K., & Jaw, K.-S. (2001). The thermal properties of KClO4 with different particle size.

609   *Thermochimica Acta*, *367–368*, 381–385. https://doi.org/10.1016/S0040-6031(00)00691-2

610   Liu, Y., Niu, S., Lai, W., Yu, T., Ma, Y., Gao, H., Zhao, F., & Ge, Z. (2019). Crystal morphology prediction of

611   energetic materials grown from solution: Insights into the accurate calculation of attachment

612   energies. *CrystEngComm*, *21*(33), 4910–4917. https://doi.org/10.1039/C9CE00848A

613   Luo, Z., Murray, B. S., Yusoff, A., Morgan, M. R. A., Povey, M. J. W., & Day, A. J. (2011). Particle-Stabilizing

614   Effects of Flavonoids at the Oil–Water Interface. *Journal of Agricultural and Food Chemistry*, *59*(6),

615   2636–2645. https://doi.org/10.1021/jf1041855

616   Macrae, C. F., Bruno, I. J., Chisholm, J. A., Edgington, P. R., McCabe, P., Pidcock, E., Rodriguez-Monge, L.,

617   Taylor, R., Streek, J. V. D., & Wood, P. A. (2008). Mercury CSD 2.0—New features for the visualization

618   and investigation of crystal structures. *Journal of Applied Crystallography*, *41*(2), 466–470.

619   https://doi.org/10.1107/S0021889807067908

620   Meenan, P. (2001). From Molecules to CrystallizersAn Introduction to Crystallization Roger Davey and John

621   Garside. Oxford University Press, New York. 2000. ISBN 0198504896. *Crystal Growth & Design*, *1*(1),

622   101–101. https://doi.org/10.1021/cg000012w

623   Metilli, L., Storm, M., Marathe, S., Lazidis, A., Marty-Terrade, S., & Simone, E. (2022). Application of X-ray

624   Microcomputed Tomography for the Static and Dynamic Characterization of the Microstructure of

625   Oleofoams. *Langmuir*, *38*(4), 1638–1650. https://doi.org/10.1021/acs.langmuir.1c03318

626   Nelson, K. M., Dahlin, J. L., Bisson, J., Graham, J., Pauli, G. F., & Walters, M. A. (2017). The Essential

627   Medicinal Chemistry of Curcumin: Miniperspective. *Journal of Medicinal Chemistry*, *60*(5), 1620–

628   1637. https://doi.org/10.1021/acs.jmedchem.6b00975

629   Pandey, K. U., & Dalvi, S. V. (2019). Understanding stability relationships among three curcumin polymorphs.

630   *Advanced Powder Technology*, *30*(2), 266–276. https://doi.org/10.1016/j.apt.2018.11.002

631   Peram, M. R., Jalalpure, S. S., Joshi, S. A., Palkar, M. B., & Diwan, P. V. (2017). Single robust RP-HPLC

632   analytical method for quantification of curcuminoids in commercial turmeric products, Ayurvedic

633   medicines, and nanovesicular systems. *Journal of Liquid Chromatography & Related Technologies*,

634   *40*(10), 487–498. https://doi.org/10.1080/10826076.2017.1329742

635   Prandini, E., Calì, E., Maloney, A. G. P., Parisi, E., & Simone, E. (2024). Predicting particle quality attributes of

636   organic crystalline materials using Particle Informatics. *Powder Technology*, *443*, 119927.

637   https://doi.org/10.1016/j.powtec.2024.119927

638   Prasad, R., Gupta, K. M., Poornachary, S. K., & Dalvi, S. V. (2020). Elucidating the Polymorphic Behavior of

639   Curcumin during Antisolvent Crystallization: Insights from Raman Spectroscopy and Molecular

640   Modeling. *Crystal Growth & Design*, *20*(9), 6008–6023. https://doi.org/10.1021/acs.cgd.0c00728

641   Preston, J. A., Parisi, E., Murray, B., Tyler, A. I. I., & Simone, E. (2024). Elucidating the Polymorphism of

642   Xanthone: A Crystallization and Characterization Study. *Crystal Growth & Design*, *24*(8), 3256–3268.

643   https://doi.org/10.1021/acs.cgd.3c01506

644   Priyadarsini, K. I. (2009). Photophysics, photochemistry and photobiology of curcumin: Studies from organic

645   solutions, bio-mimetics and living cells. *Journal of Photochemistry and Photobiology C:*

646   *Photochemistry Reviews*, *10*(2), 81–95. https://doi.org/10.1016/j.jphotochemrev.2009.05.001

647   Pugh, R. J. (2016). *Bubble and Foam Chemistry*. Cambridge University Press.

648   https://doi.org/10.1017/CBO9781316106938

649   Roelands, C. P. M., Jiang, S., Kitamura, M., ter Horst, J. H., Kramer, H. J. M., & Jansens, P. J. (2006).

650   Antisolvent Crystallization of the Polymorphs of L -Histidine as a Function of Supersaturation Ratio

651   and of Solvent Composition. *Crystal Growth & Design*, *6*(4), 955–963.

652   https://doi.org/10.1021/cg050529d

653   Sanphui, P., & Bolla, G. (2018). Curcumin, a Biological Wonder Molecule: A Crystal Engineering Point of

654   View. *Crystal Growth & Design*, *18*(9), 5690–5711. https://doi.org/10.1021/acs.cgd.8b00646

655   Sanphui, P., Goud, N. R., Khandavilli, U. B. R., Bhanoth, S., & Nangia, A. (2011). New polymorphs of

656   curcumin. *Chemical Communications*, *47*(17), 5013. https://doi.org/10.1039/c1cc10204d

657 Sarkar, A., & Dickinson, E. (2020). Sustainable food-grade Pickering emulsions stabilized by plant-based

658   particles. *Current Opinion in Colloid & Interface Science*, *49*, 69–81.

659   https://doi.org/10.1016/j.cocis.2020.04.004

660 Simone, E., & Nagy, Z. K. (2015). A link between the ATR-UV/Vis and Raman spectra of zwitterionic solutions

661   and the polymorphic outcome in cooling crystallization. *CrystEngComm*, *17*(34), 6538–6547.

662   https://doi.org/10.1039/C5CE00702J

663 Simone, E., Zhang, W., & Nagy, Z. K. (2015). Application of Process Analytical Technology-Based Feedback

664   Control Strategies To Improve Purity and Size Distribution in Biopharmaceutical Crystallization.

665   *Crystal Growth & Design*, *15*(6), 2908–2919. https://doi.org/10.1021/acs.cgd.5b00337

666 Siudem, P., Szeleszczuk, Ł., Zielińska, A., & Paradowska, K. (2023). 13C CPMAS NMR as an Alternative

667   Method to Verify the Quality of Dietary Supplements Containing Curcumin. *Molecules*, *28*(8), 3442.

668   https://doi.org/10.3390/molecules28083442

669 Tan, C., & McClements, D. J. (2021). Application of Advanced Emulsion Technology in the Food Industry: A

670   Review and Critical Evaluation. *Foods*, *10*(4), 812. https://doi.org/10.3390/foods10040812

671 Tang, J., Quinlan, P. J., & Tam, K. C. (2015). Stimuli-responsive Pickering emulsions: Recent advances and

672   potential applications. *Soft Matter*, *11*(18), 3512–3529. https://doi.org/10.1039/C5SM00247H

673 ter Horst, J. H., Deij, M. A., & Cains, P. W. (2009). Discovering New Co-Crystals. *Crystal Growth & Design*,

674   *9*(3), 1531–1537. https://doi.org/10.1021/cg801200h

675 Thorat, A. A., & Dalvi, S. V. (2014). Particle formation pathways and polymorphism of curcumin induced by

676   ultrasound and additives during liquid antisolvent precipitation. *CrystEngComm*, *16*(48), 11102–

677   11114. https://doi.org/10.1039/C4CE02021A

678 Thorat, A. A., & Dalvi, S. V. (2015). Solid-State Phase Transformations and Storage Stability of Curcumin

679   Polymorphs. *Crystal Growth & Design*, *15*(4), 1757–1770. https://doi.org/10.1021/cg501814q

680 Wu, J., & Ma, G. (2016). Recent Studies of Pickering Emulsions: Particles Make the Difference. *Small*, *12*(34),

681   4633–4648. https://doi.org/10.1002/smll.201600877

24

682 Xia, T., Xue, C., & Wei, Z. (2021). Physicochemical characteristics, applications and research trends of edible

683   Pickering emulsions. *Trends in Food Science & Technology*, *107*, 1–15.

684   https://doi.org/10.1016/j.tifs.2020.11.019

685 Xiao, J., Sarker, S. D., & Asakawa, Y. (A c. Di). (2021). *Handbook of Dietary Phytochemicals*. Springer

686   Singapore. https://doi.org/10.1007/978-981-15-4148-3

687 Yang, Y., Fang, Z., Chen, X., Zhang, W., Xie, Y., Chen, Y., Liu, Z., & Yuan, W. (2017). An Overview of Pickering

688   Emulsions: Solid-Particle Materials, Classification, Morphology, and Applications. *Frontiers in*

689   *Pharmacology*, *8*, 287. https://doi.org/10.3389/fphar.2017.00287

690 Zembyla, M., Murray, B. S., Radford, S. J., & Sarkar, A. (2019). Water-in-oil Pickering emulsions stabilized by

691   an interfacial complex of water-insoluble polyphenol crystals and protein. *Journal of Colloid and*

692   *Interface Science*, *548*, 88–99. https://doi.org/10.1016/j.jcis.2019.04.010

693 Zembyla, M., Murray, B. S., & Sarkar, A. (2018). Water-In-Oil Pickering Emulsions Stabilized by Water-

694   Insoluble Polyphenol Crystals. *Langmuir*, *34*(34), 10001–10011.

695   https://doi.org/10.1021/acs.langmuir.8b01438

696 Zembyla, M., Murray, B. S., & Sarkar, A. (2020). Water-in-oil emulsions stabilized by surfactants, biopolymers

697   and/or particles: A review. *Trends in Food Science & Technology*, *104*, 49–59.

698   https://doi.org/10.1016/j.tifs.2020.07.028

699

700

701

702

703

704

Curcumin (Cur) >78%   Demethoxycurcumin (DMC) ≈15%   Bisdemethoxycurcumin (BDMC) ≈1%
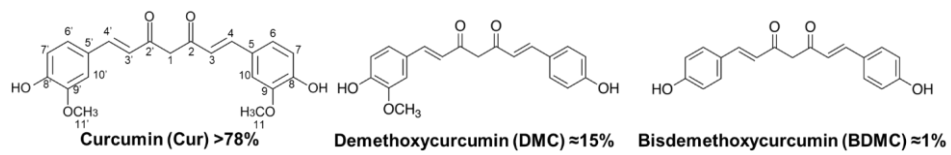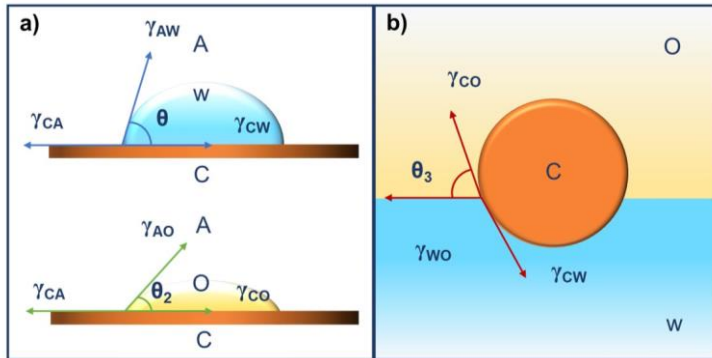
705

706   ***Figure 1:*** *Curcuminoids molecular structure and relative amount of curcuminoids in the mixture. Atom*
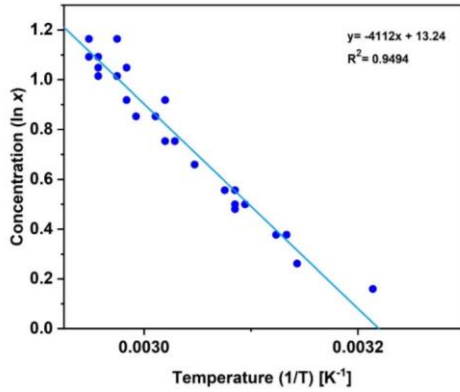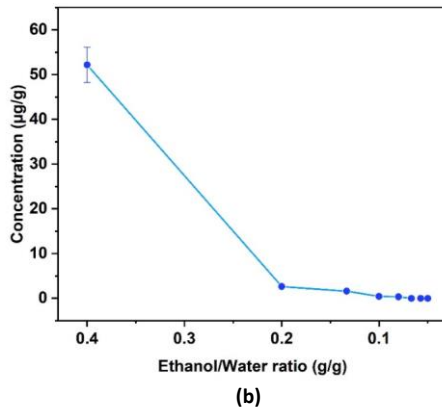707   *numbering of the keto-enolic form of curcumin is reported.*

708

709

710
711
712 **Figure 2**: Schematic of surface tensions and contact angles for air, water and curcumin and air, oil and
713 curcumin (a) and oil, water and curcumin (b)
714

715

(a)

716

(b)

717

Figure 3: *(a) Van't Hoff type plot of curcumin solubility in ethanol in the range 35-65 °C. In the y axis, concentration of curcumin as natural logarithm of the molar fraction (x), in the x axis the reciprocal of temperature in Kelvin. (b) Solubility curve of curcumin as a function of increasing water content. The amount of water increases from left to right.*

718
719
720
721

722

723

724

725

726
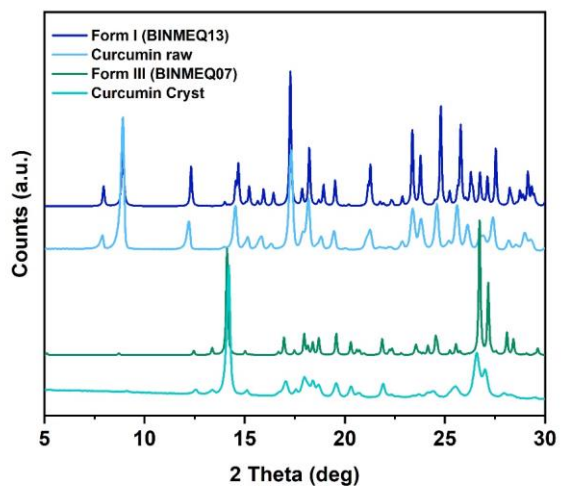
Figure 4: *PXRD pattern of raw curcumin (on the top) and recrystalized curcumin (on the bottom). The experimental pattern) are compared with the simulated pattern obtained from CSD database.*

729
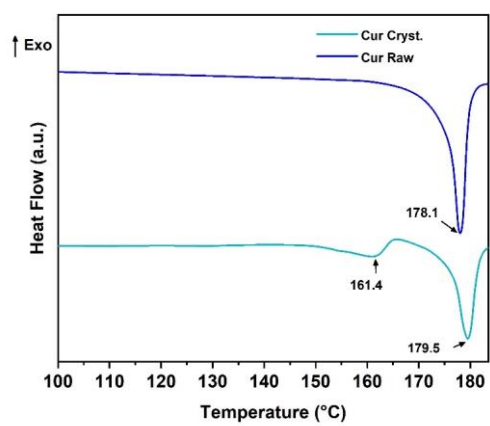
730

731   ***Figure 5:*** *DSC thermogram of raw curcumin (on the top) and recrystalized curcumin (on the bottom).*

732

733

734
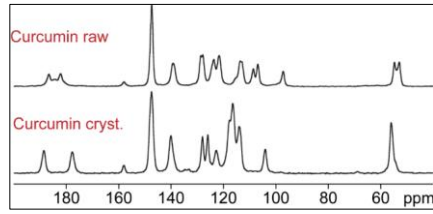
Figure 6: ^{13}C (100.63 MHz) CPMAS ssNMR spectra of the raw (top) and recrystallized curcumin (bottom) acquired at a spinning rate of 12 kHz.
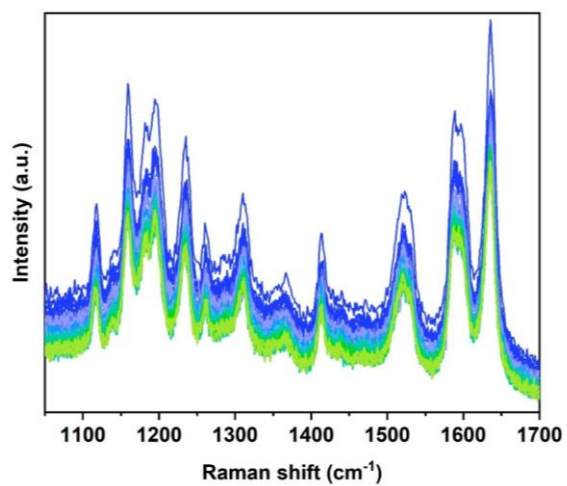
737

738
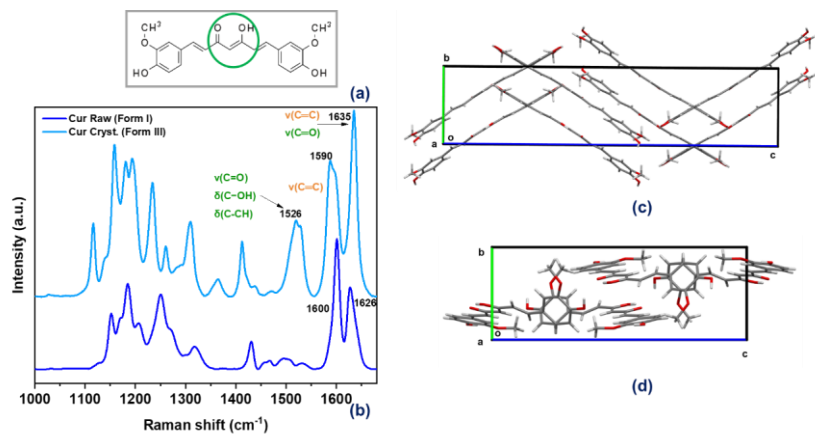
739

744

745

746

747

748

749
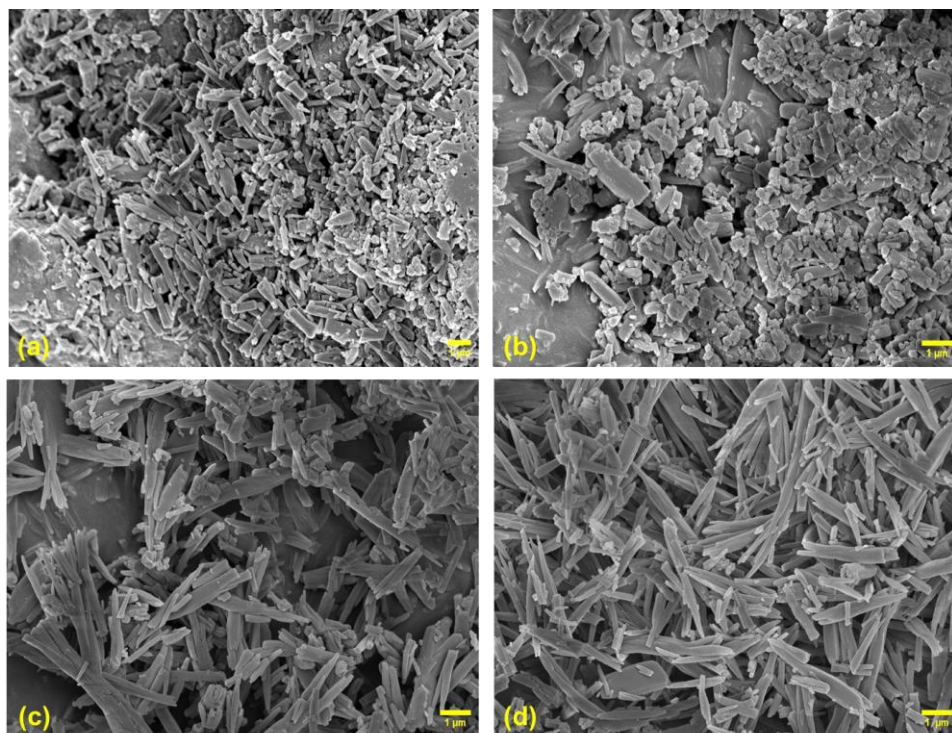

750

Figure 8: *In situ Raman spectra of recrystalized curcumin slurry in water over time. The slurry was monitored*
*for 63 hr, a total of 64 spectra were recorded*

753

754

755

756

757

Figure 9: *Recrystallized curcumin particles observed via SEM micrographs. Crystals were from Exp 1 (conditions reported in Table 1). Images were obtained with a magnification of 20 000 X, except for image (a), obtained with 15 000 X magnification. Scale bars are reported for every micrograph. (a-b) show particles with a needle/rod-like morphology; (c-d) reveals the presence of dendritic, partly broken structures.*
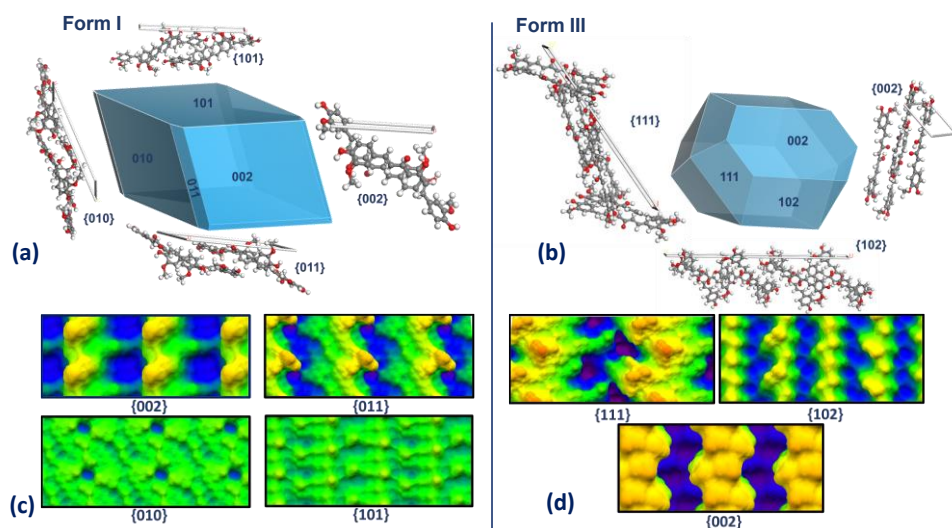
758
759
760
761

762

763
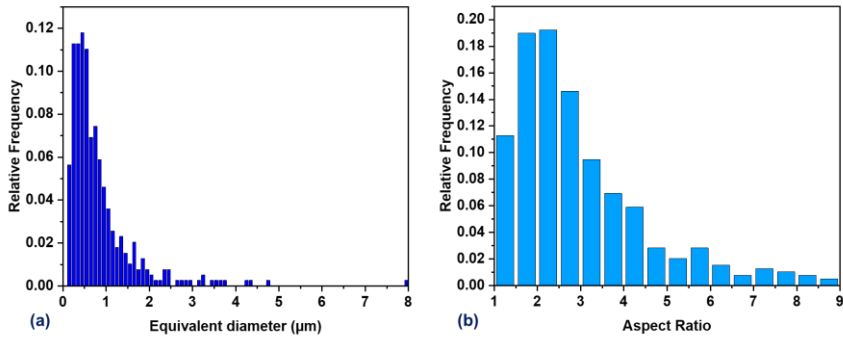
Figure 10: *Particle size and morphology distributions of a recrystalized curcumin sample. (a) Equivalent (Feret's) diameter and (b) aspect ratio of the particle population of Exp 1 (conditions reported in Table 1) were considered.*

767

Figure 11: *Morphology prediction and facet-specific topologies calculated using the attachment energy model for curcumin form I (a) and form III (b). For the two morphologies, the topology of the most dominant facets is reported. (c) and (d) show the surface analysis of the most dominant facets, expressed as the ratio between effective and projected surface. Green regions are in line with the average plane considered by calculations, while yellow/orange and blue/purple represent surfaces respectively above and below the average plane.*
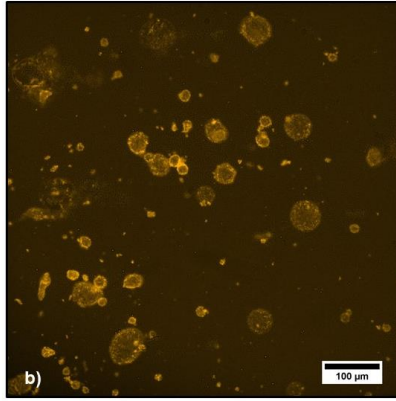
778

779

780

781
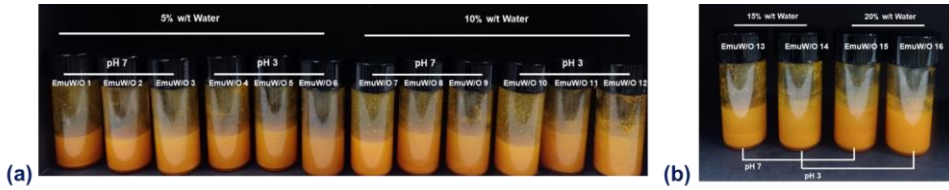
782 **Figure 12:** *W/O emulsions prepared (a) varying the mixing condition and (b) fixing the speed of agitation at*
783 *10000 rpm. The load of curcumin particles was fixed.*

784

785

786
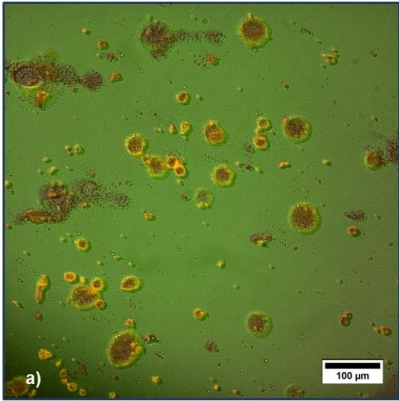
Figure 13: Confocal images of 20 wt% W/O emulsion stabilized by curcumin particles. (a) Merged channels of brightfield, green and red emission ones and(b) red channel images were collected for the same sample. The fluorescence of curcumin (both red as solid and green in MCT oil) causes the yellow colour at interfaces , whereas the green fluorescence is caused by partial dissolution of curcumin in the oil phase.

791
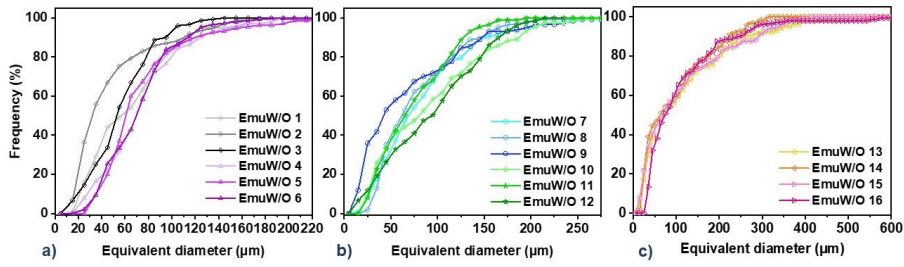
Figure 14: Emulsions droplet size distribution represented as cumulative frequency, expressed in percentage of droplet over the total number. The samples were grouped according to water content in W/O emulsions. In graph (a) emulsions prepared with 5 wt% of water can be observed,in (b) 10 wt% and (c) 15 to 20 wt% water contents are shown.

Handshaking   **Ultra-Turrax 5000**   **Ultra-Turrax 10000**

pH 7

pH 3

5 wt% Water

pH 7

pH 3

10 wt% Water

a - EmuW/O 1   b - EmuW/O 2   c - EmuW/O 3
d - EmuW/O 4   e - EmuW/O 5   f - EmuW/O 6
g - EmuW/O 7   h - EmuW/O 8   i - EmuW/O 9
j - EmuW/O 10   k - EmuW/O 11   l - EmuW/O 12

pH 7   pH 3

15 wt% Water

20 wt% Water

Ultra-Turrax 10000

m - EmuW/O 13   n - EmuW/O 14
o - EmuW/O 15   p - EmuW/O 16

805
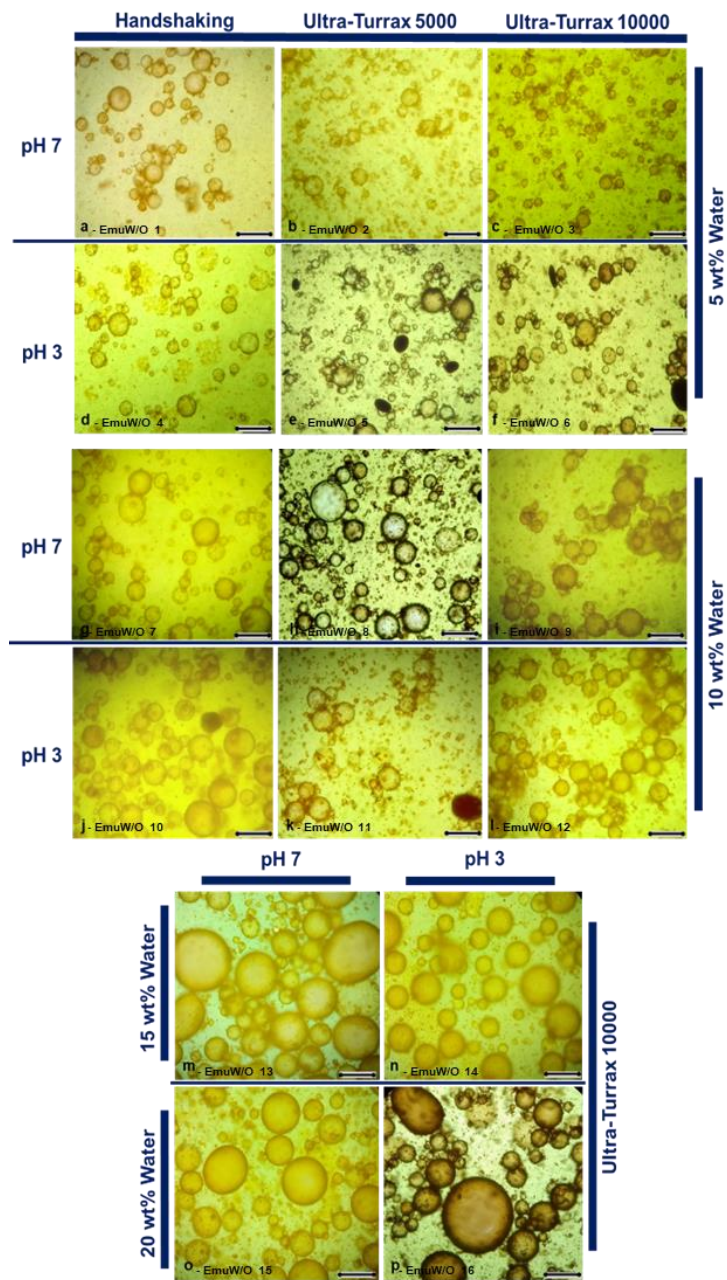
Figure 15: Images of W/O emulsion obtained through optical microscope. The scalebar is set to 250 µm for all the samples.
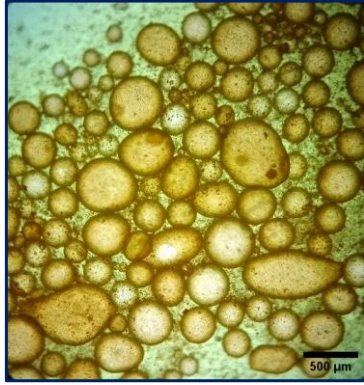
808

809   ***Figure 16****: Emulsion Emu W/O 16 after 4 months of storage. Optical microscopy reveals an enlargement of*
810   *the droplets and particle dispersed in the continuous phase.*

811

812

813

814   **Figure 17:** *Sample Emu W/O 16 left in air on a glass slide for 30 minutes. The resulting deflated structure*
815   *demonstrates that the particles are strongly adsorbed at the interface.*

816

817

818
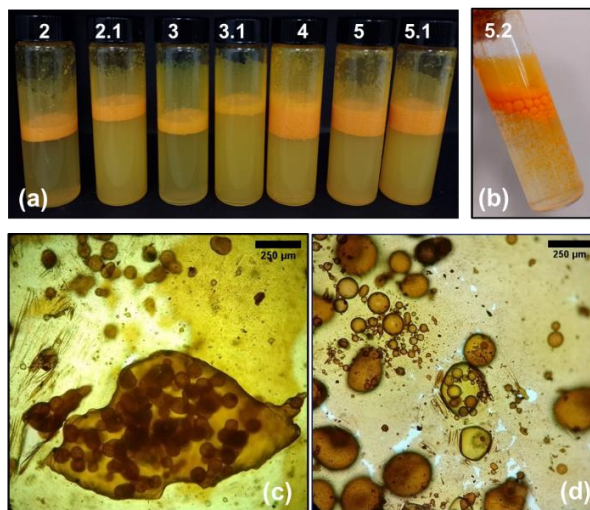
Figure 18: In O/W emulsions from 2 to 5.1 reported (a) water at pH 7 was used while (b) 5.2 sample was prepared with water at pH 3. Images obtained through optical microscope of sample 2 (c) and sample 5.1 (d) are reported.

822

823
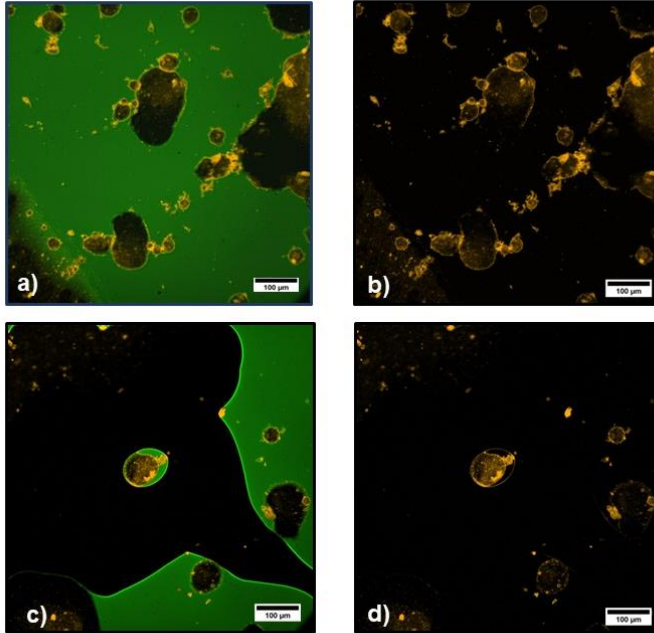
Figure 19: *confocal images of sample Emu O/W 5. The auto-fluorescence of curcumin causes the yellow brightness. Green fluorescence is caused by partial dissolution of curcumin in the oil phase. Images (b) and (d) show curcumin only autofluorescence. Images a) and c) were obtained in brightfield option.*

829

Table 1: *List of the experiments performed. DoE approach was used. The four factors and the five levels were first combined in a full factorial design, for a total amount of 625 experimental points. ccdesign function was then applied to select the experiments from the experimental domain.*

Experiment #	Concentration (mg/g)	EtOH/Water Ratio	Water volume (ml)	Speed mixing (rpm)
Exp 1	7.25	01:12.5	445	14900
Exp 2	7.25	01:12.5	445	18300
Exp 3	7.25	01:12.5	615	14900
Exp 4	7.25	01:12.5	615	18300
Exp 5	7.25	01:17.5	445	14900
Exp 6	7.25	01:17.5	445	18300
Exp 7	7.25	01:17.5	615	14900
Exp 8	7.25	01:17.5	615	18300
Exp 9	11.07	01:12.5	445	14900
Exp 10	11.07	01:12.5	445	18300
Exp 11	11.07	01:12.5	615	14900
Exp 12	11.07	01:12.5	615	18300
Exp 13	11.07	01:17.5	445	14900
Exp 14	11.07	01:17.5	445	18300
Exp 15	11.07	01:17.5	615	14900
Exp 16	11.07	01:17.5	615	18300
Exp 17	5.85	01:15	530	16600
Exp 18	13.58	01:15	530	16600
Exp 19	9.04	01:10	530	16600
Exp 20	9.04	01:20	530	16600
Exp 21	9.04	01:15	360	16600
Exp 22	9.04	01:15	700	16600
Exp 23	9.04	01:15	530	13200
Exp 24	9.04	01:15	530	20000
Exp 25	9.04	01:15	530	16600
Exp 22	9.04	01:15	700	16600
Exp 23	9.04	01:15	530	13200
Exp 24	9.04	01:15	530	20000
Exp 25	9.04	01:15	530	16600

830

831 **Table 2:** *Experimental condition tested for the preparation of W/O emulsions*

Experiment #	Oil (g)	Water (g)	pH	Curcumin (mg)	Mixing (rpm)
Emu W/O 1	4.73 (94.6 wt%)	0.25 (5 wt%)	7	20 (0.4 wt%)	Handshaking
Emu W/O 2	4.73 (94.6 wt%)	0.25 (5 wt%)	7	20 (0.4 wt%)	Ultra-Turrax 5000
Emu W/O 3	4.73 (94.6 wt%)	0.25 (5 wt%)	7	20 (0.4 wt%)	Ultra-Turrax 10000
Emu W/O 4	4.73 (94.6 wt%)	0.25 (5 wt%)	3	20 (0.4 wt%)	Handshaking
Emu W/O 5	4.73 (94.6 wt%)	0.25 (5 wt%)	3	20 (0.4 wt%)	Ultra-Turrax 5000
Emu W/O 6	4.73 (94.6 wt%)	0.25 (5 wt%)	3	20 (0.4 wt%)	Ultra-Turrax 10000
Emu W/O 7	4.48 (89.6 wt%)	0.5 (10 wt%)	7	20 (0.4 wt%)	Handshaking
Emu W/O 8	4.48 (89.6 wt%)	0.5 (10 wt%)	7	20 (0.4 wt%)	Ultra-Turrax 5000
Emu W/O 9	4.48 (89.6 wt%)	0.5 (10 wt%)	7	20 (0.4 wt%)	Ultra-Turrax 10000
Emu W/O 10	4.48 (89.6 wt%)	0.5 (10 wt%)	3	20 (0.4 wt%)	Handshaking
Emu W/O 11	4.48 (89.6 wt%)	0.5 (10 wt%)	3	20 (0.4 wt%)	Ultra-Turrax 5000
Emu W/O 12	4.48 (89.6 wt%)	0.5 (10 wt%)	3	20 (0.4 wt%)	Ultra-Turrax 10000
Emu W/O 13	4.23 (84.6 wt%)	0.75 (15 wt%)	7	20 (0.4 wt%)	Ultra-Turrax 10000
Emu W/O 14	4.23 (84.6 wt%)	0.75 (15 wt%)	3	20 (0.4 wt%)	Ultra-Turrax 10000
Emu W/O 15	3.98 (79.6 wt%)	1 (20 wt%)	7	20 (0.4 wt%)	Ultra-Turrax 10000
Emu W/O 16	3.98 (79.6 wt%)	1 (20 wt%)	3	20 (0.4 wt%)	Ultra-Turrax 10000

832

833

Table 3: *Experimental condition tested for O/W emulsions*

Experiment #	Oil (g)	Water (g)	Curcumin (mg)	Mixing (rpm)	
				Dispersion	**Emulsification**
Emu O/W 2	0.63 (5.2 wt%)	11.53 (94.7 wt%)	12.5 (0.1 wt%)	Ultra-turrax 10000 (3 min)	Ultra-turrax 10000 (1min)
Emu O/W 2.1	0.75 (5.2 wt%)	14.25 (94.7 wt%)	15 (0.1 wt%)	Ultra-turrax 4000 (5 min)	Ultrasound bath (2 min 40kHz) + Handshaking (1 min)
Emu O/W 3	0.63 (5.2 wt%)	11.53 (94.7 wt%)	6.25 (0.05 wt%)	Ultra-turrax 10000 (3 min)	Ultra-Turrax 10000 (1min)
Emu O/W 3.1	0.75 (5.2 wt%)	14.25 (94.7wt%)	7.5 (0.05 wt%)	Ultra-Turrax 4000 (5 min)	Ultrasound bath (2 min 40kHz) + Handshaking (1 min)
Emu O/W 4	0.75 (5 wt%)	14.25 (95 wt%)	45 (0.3 wt%)	Ultra-Turrax 4000 (5 min)	Ultrasound bath (2 min 40kHz) + Handshaking (1 min)
Emu O/W 5	1.5 (10.5 wt%)	12.75 (89.3 wt%)	15 (0.1 wt%)	Ultra-Turrax 4000 (5 min)	Ultrasound bath (2 min 40kHz) + Handshaking (1 min)
Emu O/W 5.1	1.5 (10.5 wt%)	12.75 (89.4wt%)	15 (0.1 wt%)	Ultra-Turrax 4000 (5 min)	Ultrasound bath (2 min 40kHz) + Ultraturrax 10000 (1 min)
Emu O/W 5.2	1.5 (10.5 wt%)	12.75 (89.4wt%) (pH 3)	15 (0.1 wt%)	Ultra-Turrax 4000 (5 min)	Ultrasound bath (2 min 40kHz) + Handshaking (1 min)

834

835

836

837   *Table 4:* ^{13}C *chemical shifts of signals C2 and C2' for the three known curcumin polymorphs* (Dai et al., 2020).

^{13}C CPMAS SSNMR – Chemical shift (δ, ppm)

	Form I	Form II	Form III
C2	187.4	189.6	190.2
		186.2	
C2'	182.7	179.2	177.8
		177.8	

838

839

840

841 **Table 5:** *Attachment energy calculation, surface roughness and percentage areas of the most dominant*
842 *facets relative both to curcumin polymorphs form I and form III.*

	hkl	dhkl	Eatt (Total) (kcal mol^{-1})	Eatt (vdW) (kcal mol^{-1})	Eatt (Electrostatic) (kcal mol^{-1})	Eatt (H-bond) (kcal mol^{-1})	% Total facet area	Roughness
Form I	{101}	11.11	-63.9	-61.3	0	-2.6	5.1	1.244
	{101}	10.25	-26.8	-25.5	0	-1.3	42.4	1.196
	{002}	9.92	-40.8	-39.5	0	-1.3	24.2	1.780
	{010}	7.18	-45.3	-44.3	0	-1.0	23.1	1.627
Form III	{002}	17.23	-104.3	-61.5	-27.6	-15.2	30.7	1.686
	{102}	10.14	-130.5	-67.1	-27.6	-35.9	35.2	2.980
	{111}	6.61	-178.4	-113.5	-36.7	-28.3	34.1	1.693

843

844

845

Table 6: *The contact angle values for raw curcumin and recrystalized curcumin are reported. Water at pH 7, pH 3 (adjusted with HCl 0.1M) and MCT oils were tested.*

	Water (ϑ_1 pH 7)	Water (ϑ_1 pH 3)	Oil (ϑ_2)
Cur Raw (Form I)	90.0 ° ± 5.0°	84.3° ± 10.3°	29.0° ± 0.7°
Cur (Form III)	62.4° ± 6.4°	63.3° ± 1.9°	24.4° ± 2.5°

846

847

848

849

850

851

Table 7: *Mean droplet size (diameter) and standard deviation (S.D.) calculated from images analysis using ImageJ software, as reported above for particle size distribution. The wide range of dimensions is due to the formation of smaller droplets which create a nest that stabilize bigger droplets through bridging mechanism.*

852

	Mean (µm)	S.D. (µm)
1	68.83	38.07
2	51.75	38.97
3	60.45	27.48
4	78.40	38.01
5	77.16	39.46
6	75.64	30.68
7	87.32	53.78
8	81.52	46.26
9	71.75	60.09
10	95.74	61.86
11	97.60	40.81
12	97.13	54.04
13	119.20	109.77
14	100.44	82.05
15	114.11	103.88
16	115.81	106.89

853